LA-UR -93-370

LA-UR--93-370

DE93 007330

Los Alamos National Laboratory is operated by the University of California for the United States Department of Energy under contract W-7405-ENG-36

TITLE Laser Desorption in an Ion Trap Mass Spectrometer

AUTHOR(S) G. C. Eiden, M. E. Cisper, M. L. Alexander, P. H. Hemberger, and N. S. Nogar

SUBMITTED TO OE LASE '93, Los Angeles, CA, 1/17-22/93

DISCLAIMER

Los Alamos Los Alamos National Laboratory
Los Alamos, New Mexico 87545

FORM NO. 836 R4
ST. NO. 2629 5/81

Laser desorption in an ion trap mass spectrometer

G. C. Eiden, M. E. Cisper, M. L. Alexander, P. H. Hemberger, and N. S. Nogar

Chemical and Laser Sciences Division
Los Alamos National Laboratory
Los Alamos, NM. 87545

ABSTRACT

Laser desorption in a ion-trap mass spectrometer shows significant promise for both qualitative and trace analysis. Several aspects of this methodology are discussed in this work. We previously demonstrated the generation of both negative and positive ions by laser desorption directly within a quadrupole ion trap. In the present work, we explore various combinations of d.c., r.f., and time-varying fields in order to optimize laser generated signals.

In addition, we report on the application of this method to analyze samples containing compounds such as amines, metal complexes, carbon clusters, and polynuclear aromatic hydrocarbons. In some cases the ability to rapidly switch between positive and negative ion modes provides sufficient specificity to distinguish different compounds of a mixture with a single stage of mass spectrometry. In other experiments, we combined intensity variation studies with tandem mass spectrometry experiments and positive and negative ion detection to further enhance specificity.

2. INTRODUCTION & BACKGROUND

The coupling of laser desorption with mass spectral detection has produced a powerful method for the analysis of complex liquid and solid samples,[1-6] and has found diverse areas of application, from analysis of superconductors[7] to complex biomolecules.[8] This process typically involves the direct production of ionized species as a result of the interaction of a high power, $\geq 10^6$ Watts/cm^2, laser pulse with a solid surface, matrix, or sample adsorbed on the surface.[9, 10] The result is the formation of a neutral plasma containing positive ions, neutral species, electrons, and negative ions.[11] The high heating rates[12] (10^{10} K/sec) and short irradiation times[13] (nanoseconds) permit the desorption of thermally labile or high molecular weight molecules with little or no thermal degradation.[14, 15]

Laser desorption/ionization techniques have been combined with virtually all types of mass analyzers, including sector,[16, 17] time-of-flight,[18-20] quadrupole,[21, 22] tandem[17, 23] and ion storage mass spectrometers, including ion cyclotron resonance[24-26] and quadrupole ion traps.[5, 27, 28] Because of the relatively low duty cycle associated with many pulsed lasers, typically 10 Hz-1 kHz, most work has been done with mass spectrometers which allow for multiplex detection—the interrogation of a large mass range on each shot. Because of their potentially higher resolution, ion cyclotron resonance (ICR) and quadrupole ion traps (ITMS) are often used in preference to time-of-flight instruments.

The combination of laser desorption/ionization techniques with trapped ion methodologies (ICR and ITMS) provides an easy route to combine several spectroscopic and mass spectrometric techniques into a single analytical sequence. Lasers have long been used with ion cyclotron resonance (ICR) mass spectrometers for desorption[29, 30] and for photodissociation studies.[31] The combination of lasers with ion trap mass spectrometers is a more recent development. Early experiments used a quadrupole ion storage device (QUISTOR) with a quadrupole mass filter for fundamental studies of ion spectroscopy.[32, 33] More recently, laser desorption techniques have been performed with ITMS detection.

Table 1. Published research in laser desorption/ionization ion trap mass spectrometry.

Laser Parameters	Geometry	Timing (laser fires)	Result	Source
CO_2/10 μm ≈100 nsec 10^6 W/cm^2	through ring electrode; sample flush with ring	start of rf storage voltage	amines, peptides, sugars; LD plus EI	39
Nd:YAG /1.06 μm ≈20 nsec 10^6 W/cm^2?	through ring electrode; sample flush with ring	during storage voltage; variable delay to analysis	$N(C_6H_5)(CH_3)_3Cl$; dependence on rf amplitude, pressure; MS/MS	40
Nd:YAG /1.06 μm ≈10 nsec Fiber-optic coupling	ions formed external to trap; z-axis injection	near end of storage period	Au^+, Cs^+, Cs_2I^+, Ta^+, TaO^+;	41
Nd:YAG /1.06 μm ≈10 nsec 10^9 W/cm^2	through ring electrode; sample flush with ring	during storage voltage	analysis of μ-particles; silicon carbide, phosphonium salts	42
Nd:YAG /1.06 μm ≈10 nsec 10^9 W/cm^2	through ring electrode; sample flush with ring	during storage voltage	production of cluster isobars for high-precision spectrometry; $^{12}C_7$; $^{28}Si_3$	43
Nd:YAG /1.06 μm ≈10 nsec 10^9 W/cm^2	through ring electrode; sample flush with ring	during storage voltage	analysis of metal alloys; Cu^+, Zn^+, Cd^+, Sn^+, Ag^+	5
Nd:YAG /1.06 μm ≈20 nsec 10^9 W/cm^2	ions formed externally; simultaneous z, r-axis injection	during storage voltage; collisional stopping of ions in trap	production of low energy (≤1 meV) W^{+1-4}, Mo^{+1-6}; charge transfer reactions	44, 45
Nd:YAG 0.532 μm ≈10 nsec 10^8 W/cm^2?	through ring electrode; sample outside ring	prior to applied trapping potential	positive and negative carbon cluster ions simultaneously stored	38
Nd:YAG 1.06/0.532 μm ≈10 nsec 10^6-10^8 W/cm^2	ions formed externally, fiber-optic coupling; z-axis injection	during storage voltage	crown ethers, digitoxigenin tetraphenylporphine, gramicidine S	46
XeCl excimer 308 nm, ≈ 10 nsec ≈10^7 W/cm^2	through ring electrode; sample flush with ring	laser fires on rising edge of trapping potential	$N(C_8H_5)(CH_3)_3I$; dependence on rf, dc amplitude, pressure.	this work

In this manuscript, we review briefly previous results in laser desorption with quadrupole ion traps, and present recent results from our laboratory on the use of 308 nm XeCl excimer laser desorption in the Finnigan Ion Trap Mass Spectrometer.

Table 1 provides a summary of recent results in laser desorption/ionization ion trap mass spectrometry. These efforts point to a number of interesting results. First, there has been relatively little work done in this field, compared to the enormous volume in laser ablation TOF/MS or even the significant literature in ICR/MS. The efforts listed in this table represent a significant fraction of all published work in this area. Much of the work reported here is in methods development, another indication of the relative youth of this technique. Although there have been a number of geometries, and a wide span of experimental parameters used in laser ablation ITMS experiments, there is still much to be understood, and substantial opportunity for improvement.

A fundamental problem lies in stopping and trapping ions in the ion trap. The applied rf voltage produces a substantial effective potential barrier for injection of ions into the trap. In general, ions either have insufficient energy to enter the trap or, if they do, they will penetrate and pass through the trap, over the top of the potential barrier on the other side. Debye shielding of the ion cloud may partially compensate for this problem[34]; electrons ejected with the ions may partially shield the cloud from the full effect of the potential barrier. After entry, the electrons find themselves in unstable orbits, and are immediately ejected, while the naked ions are left with insufficient energy to leave the trap. Additional assistance may be provided by collisional processes within the trap, which will reduce slightly the kinetic energy of injected ions, damp their motion, and increase the probability of trapping.

Several authors have explored theoretically the possibility of increasing the trapping efficiency by gating the rf-potential "on" after the ions have been generated and entered the trap[35-37]. Prior to our work, only one of the experimental studies[38] described in Table 1 has reported this configuration, however, and in that case no systematic study of parameters was attempted. *In this work we describe the use of carefully timed laser ablation together with intrinsic time constants in the Finnigan ITMS apparatus to improve the trapping efficiency.* In addition, we present survey laser desorption mass spectra obtained in a number of different systems, including amines, metal complexes, carbon clusters, and polynuclear aromatic hydrocarbons.

3. EXPERIMENTAL

The combined laser/ion trap apparatus has been previously described and is only briefly outlined here. A unique ion trap mass spectrometer system that incorporates an ion optical/laser optical platform within a large (1 m diam) vacuum chamber was developed and built for these experiments. The apparatus is based on a Finnigan ITMS and a Questek XeCl excimer laser. Details of this experiment may be found elsewhere[Hemberger, et al, 1992]. The ion trap control and detection electronics are standard Finnigan components. A Phrasor Model G61 channel electron multiplier with conversion dynode was used for positive/negative ion detection. Biasing the conversion dynode to approximately +4 kV allows for the detection of negative ions in a fashion similar to that previously described. The ion trap was modified for desorption experiments by drilling opposed (180°) 2.5 mm holes in the ring electrode as described previously[39]. A sketch of the ionization region is shown in Figure 1.

Samples were introduced to the ion trap with a direct insertion probe guided through one of the holes. The surface of the probe tip (2.2 mm diam.) was flush with the inner surface of the ring electrode and the material on the probe tip was desorbed by the laser beam which passed through the opposite hole. The probe tip material most often used was 304L stainless steel although a Macor tip was used for experiments with metal complexes. Helium, at an uncorrected ion gauge pressure of 1-2 x 10^{-5} Torr, was used as a buffer gas in most experiments.

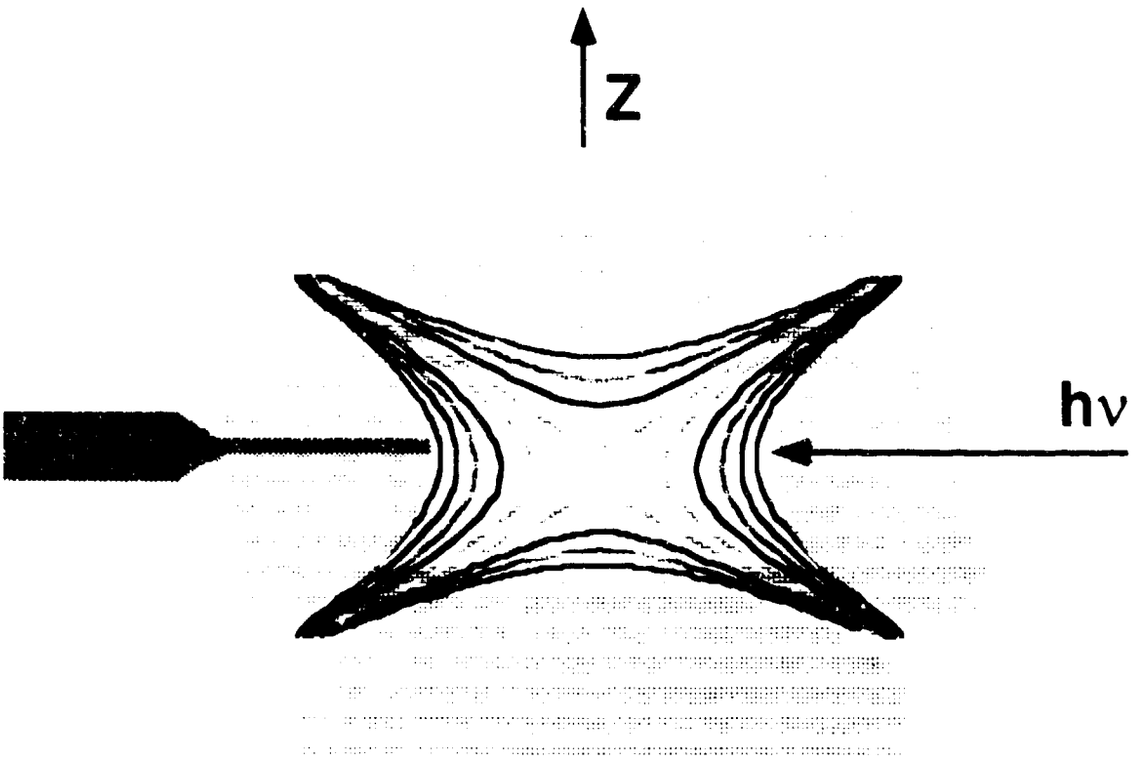

Figure 1 shows a schematic of the trapping region. Electrodes are represented in gray; the sample probe is inserted from the left, and the laser beam is incident from the right. Approximate equipotential field lines are also shown.

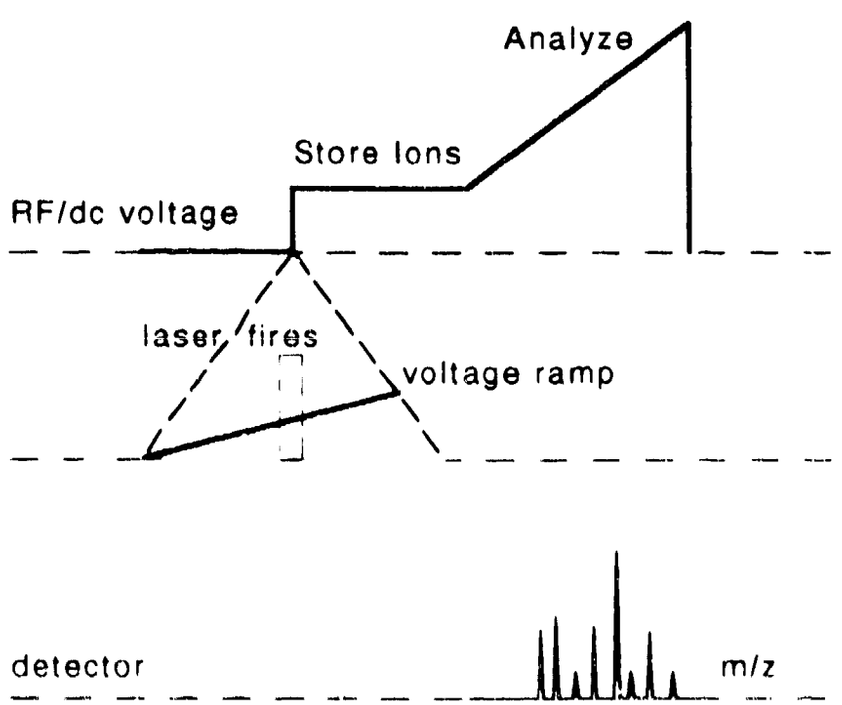

Figure 2. Depicts the timing sequence for mass spectral analysis by laser ablation ITMS. The horizontal axis represents time; the expanded region in the middle trace shows that the voltage rise is not instantaneous, but has a finite time constant associated with the apparatus

The XeCl excimer laser (Questek 2200) laser produced output pulses with a 15 ns duration at 308 nm. The beam was focused by a 60 cm lens, and the size of the laser beam at the probe tip was found to be 1x2 mm, and Gaussian in the z-direction, as measured with a Reticon photodiode array on an equivalent beam line. Laser energy at the probe tip was typically ≥1 mJ/pulse, corresponding to a power density of $\geq 3 \times 10^6$ Watt/cm^2. Timing was controlled with a Stanford Research model 535 digital delay/pulse generator, which was triggered by a pulse generated at the start of the data acquisition sequence by the ITMS electronics. Much of the data shown here were taken by firing the laser during the rising edge of the trapping rf potential, as shown in Figure 2, and at random phase with respect to the fundamental RF.

4. RESULTS

4.1 Time-dependent Trapping

Trimethylphenyl ammonium iodide was examined first as a benchmark compound. Initial laser desorption ion trap mass spectra of this compound were obtained by firing the laser during application of the trapping potential, and were in qualitative agreement with previous work[40]. Cation peaks were observed at m/z of 136 (the intact cation), as well as at lower and higher masses (see below); in addition, the iodide ion was also observed. A logarithmic plot of ion current vs. He pressure was approximately linear over a range from 10^{-6} to 10^{-3} Torr. These data were acquired with by firing the laser during the trapping potential, and with a delay of ≈20 ms between laser shot and the beginning of the mass scan.

The power dependence for the creation of positive ions and negative ions (I^-) from trimethylphenyl ammonium iodide (TMA) at 308 nm is shown in Figure 3. Cation signal, shown by the solid circles, is the sum of all positive ion peaks to include the contributions of lower mass fragments which become more abundant at higher laser energies. The only negative ion observed from this compound was I^-, which was approximately 20 times less abundant than the sum of the cations. This disparity may be a function of the reduced Debye shielding afforded negative ions by accompanying electrons. Both cations and anions appear to have approximately the same threshold, although they may exhibit slightly different power laws. The increase is rapid and smooth for laser energies above 1 mJ/pulse; most data discussed below were acquired at 1.5-2.0 mJ/pulse.

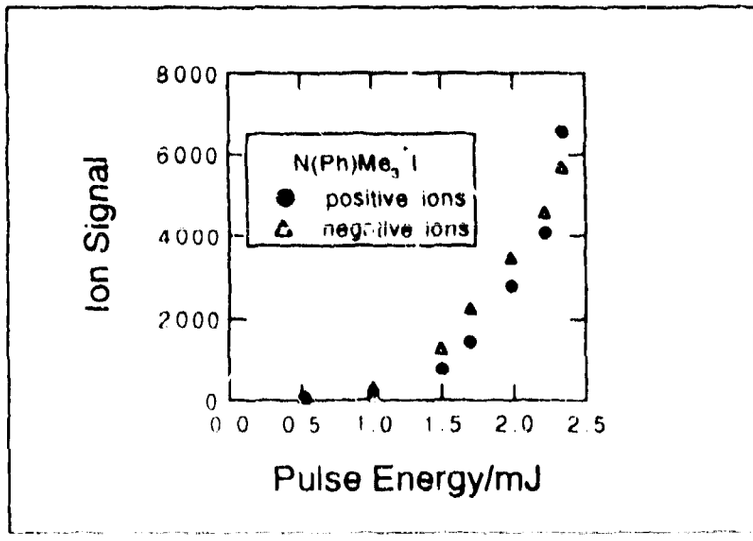

Figure 3 shows the threshold signal (left) for a neat sample of trimethyl-phenyl ammonium iodide

We then explored the effect of timing between the laser ablation event and various combinations of d.c., r.f., and time-varying fields in order to optimize the observed signal. In, general, it was found that firing the laser on the increasing edge of the rf-trapping potential (and including in some cases, a d.c. component), as shown in Figure 2, significantly increased the observed signal level, relative to firing the laser either before the application of

the trapping potential, or after the potential has been fully developed. Typical results are shown in Figure 4, below. Here the detected signal for several masses is plotted as a function of delay between initiation of the rf potential and firing the laser. The higher masses (m/e≥136) correspond to the combination of various fragments with the parent ion.

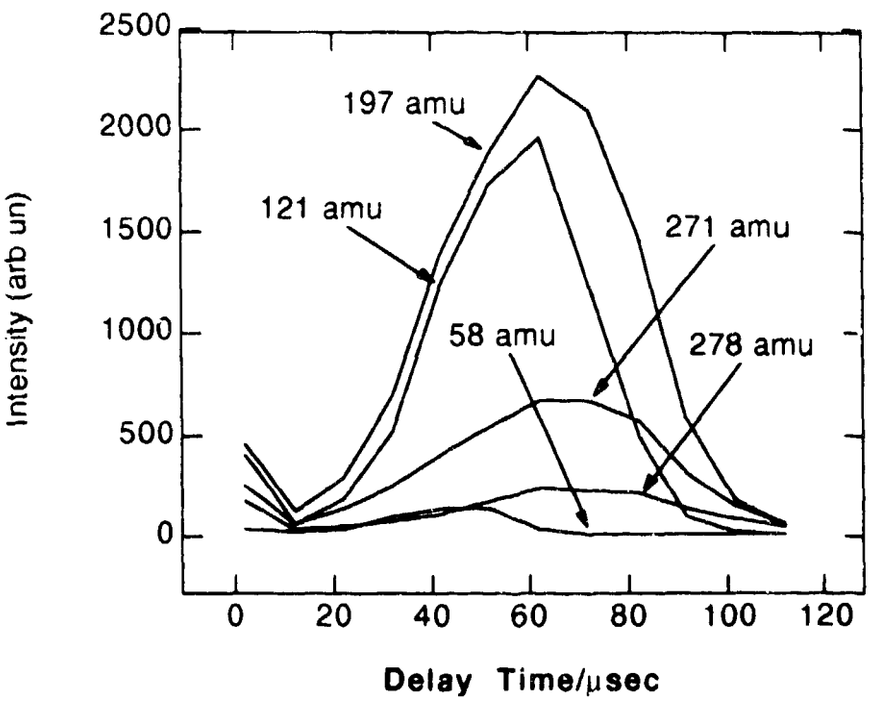

Figure 4 shows the signal detected for several ions as a function of delay between initiation of the rf trapping potential and firing the ablation laser. This data was obtained with the rf potential ramped to a final voltage (≈508 V) which ensured ejection (and hence, no detection) of ions below a mass of 40 au.

In general, these signals peak in the delay time range 40-100 μsec; independent measurements have shown that the rf potential rises with a time constant of ≈100 μsec. Thus most of the data shown above were acquired during this rise period. Generation of ions during the rise time of the rf clearly has significant advantages, relative to most previous experiments (see Table 1), where laser was not fired until the trapping potential was fully developed.

This can be understood in a qualitative sense by considering Figure 5, which shows temporal development of the effective rf potential on a trajectory initiating at the sample probe, and normal to its surface. Early in the formation of the electric field, the magnitude is small, so that an ion is presented with a relatively low barrier to entry into the trap, and a high probability of entry. During the time that the ion is traversing the trap (typically at least 100 μsec), the amplitude of the field increases, and the ion is presented with much larger barrier to escape from the trap. Thus the probability of trapping is increased.

In order to quantify this more clearly, additional data was obtained. Figure 6 shows the time delay for which the peak signal occurs, T_{max}, for a number of different masses, as a function of the rf trapping potential. This potential is expressed in terms of the lowest mass ion for which stable trajectories are available in the ion trap. In general, the best trapping potential occurs at slightly longer delays for heavier ions. This also corresponds to higher

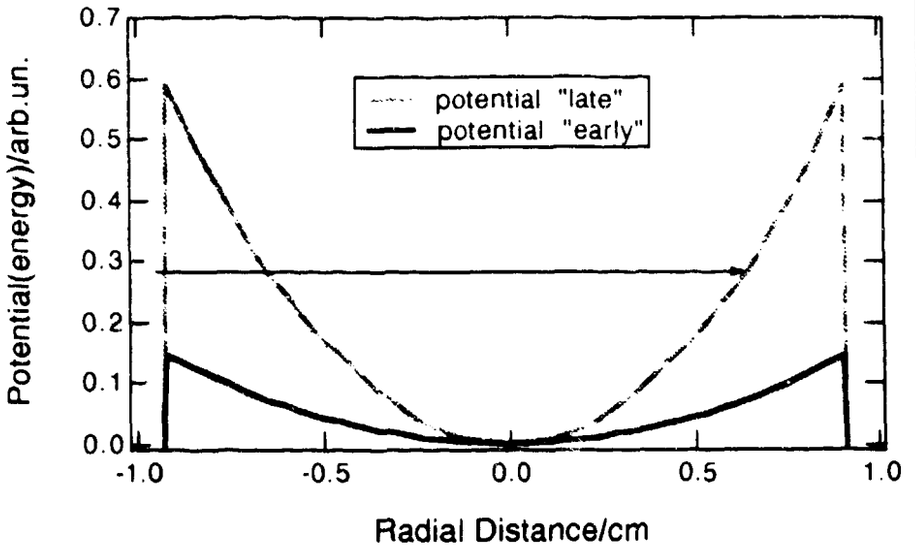

Figure 5. Shows the effective electric field experienced by a point charge on a linear trajectory from the sample probe across the trap, both "early" and "late" in the rise of the trapping potential. Also shown is one possible translational energy for an ion ejected from the probe surface. Note that because the potential rises during transit, the ion is able to surmount the entry barrier, but not the exit barrier.

effective potentials, since the rf field is closer to reaching its steady state at long delay times. This is reasonable, since the heavier ions are likely to have somewhat greater energies, will be able to penetrate a larger entrance barrier, and will need a higher exit barrier to ensure trapping. The difference in energies between light and heavy ions is due to a fundamental aspect of laser desorption; this process usually produces imparts similar velocities to all components leaving the surface[47-49], due to the high frequency of collisions in the near-surface region. The high-mass species therefore obtain higher energies.

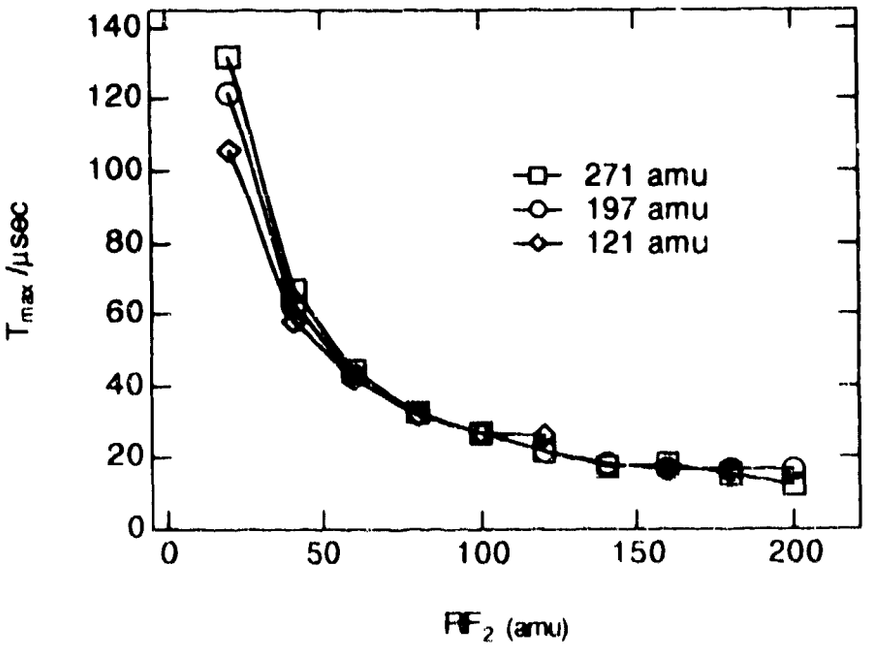

Figure 6 shows the delay time for maximum signal, T_{max}, as a function of rf trapping potential for ions having m/z's as indicated in the legend.

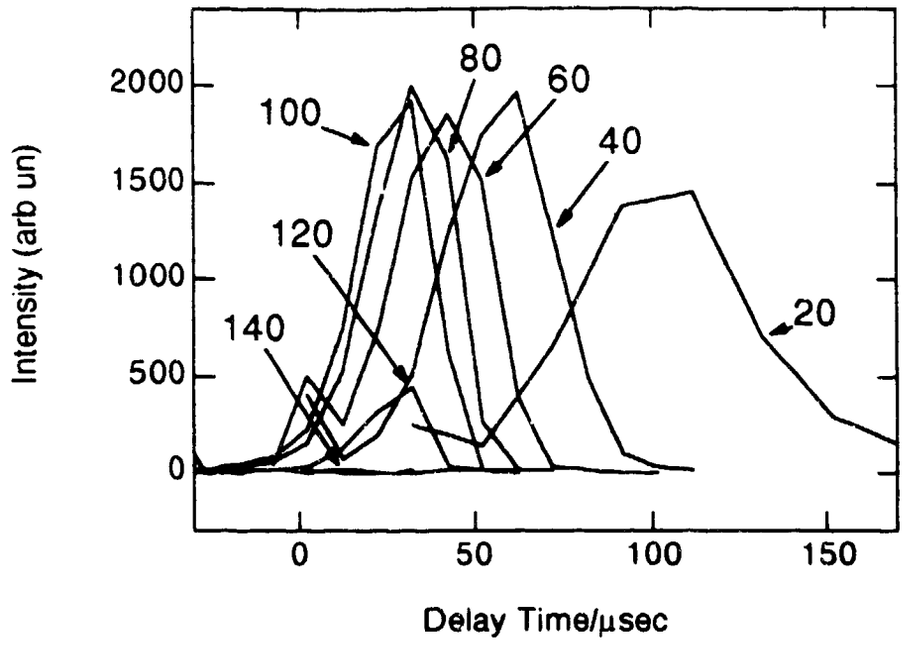

Figure 7 shows the mass 121 signal as a function of delay time for various trapping potentials (expressed as the minimum mass which can be stored at a given potential).

Lastly, in Figure 7 we show the intensity for the m/z=121 signal as a function of delay time for several rf potentials. It should be noted that in most previous experiments (Table 1), the laser was not fired until many milliseconds after the trapping potential had been applied; typically this potential corresponded to a lower mass of ≈20-40. By this time, our signals have reduced to a very small fraction of the value exhibited at optimal delay times. *Thus the signal observed by triggering on the leading edge of the rf field is at least an order of magnitude larger than that observed by firing the laser after the rf field is fully formed.*

4.2 Applications in Chemical Analysis

We previously have demonstrated the generation of both negative and positive ions by laser desorption directly within a quadrupole ion trap and the application of this method to analyze complex samples containing compounds such as explosive residues, metal complexes, and polynuclear aromatic hydrocarbons, and carbon clusters[50]. In initial experiments, 2 μl of a Supelco PAH standard was deposited on the probe tip. The negative ion signal was in general larger than the positive ion signal for these compounds, reflecting their significant electron affinities. In addition, we observed interesting laser pulse energy-related effects, as depicted in Figure 8. At low laser energies, or for electron impact ionization of thermally vaporized sample, only monomers and fragments where observed, as shown in the left of this figure. At higher laser energies, the spectra also included peaks at masses (c.f. ≈ m/z=305) corresponding to various proton-bonded dimers, as shown on the right side of the figure. The production of complexes and clusters can be attributed to the relatively high densities of ions, neutrals and electrons generated above the probe surface at high laser intensities. This dramatically increases the probability of collisional processes leading to ion-molecule reactions.

Laser desorption mass spectra were also obtained for carbon clusters, including various of the fullerene-type molecules, as shown in Figure 9. These spectrum were obtained in an effort to determine whether these molecules contained encapsulated lanthanide ions. The mass spectral evidence clearly indicates that they do not. The spectrum is dominated by the C_{60} and C_{70} peaks, with minor signal at masses corresponding to the loss (or gain) of C_4 units from the parents.

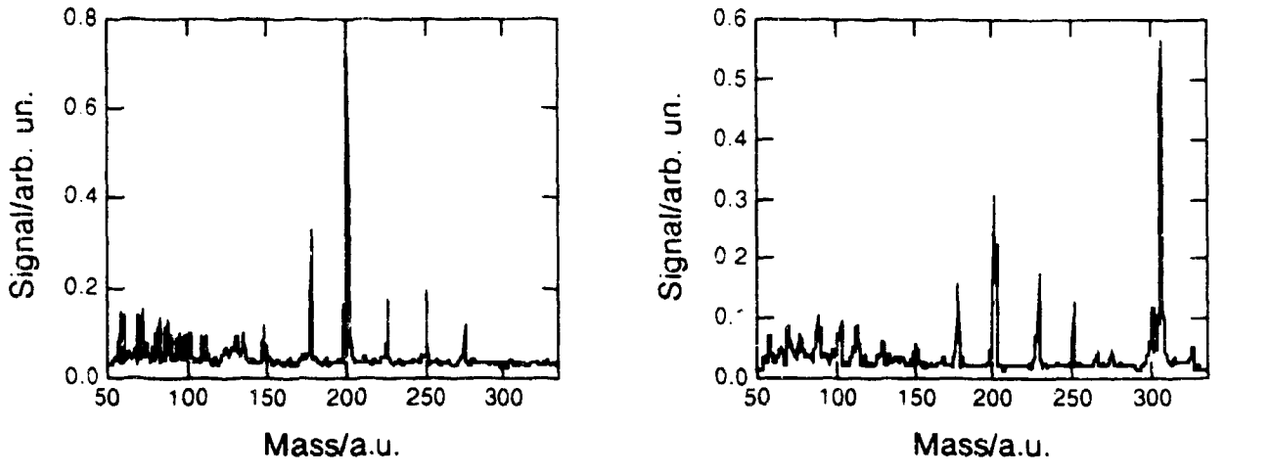

Figure 8 shows positive ion mass spectra from a mixture of PAH's. At left, the electron impact spectrum shows only monomeric units and fragments, while the figure on the right also shows signal at a mass corresponding to a proton-bonded dimer.

Additional experiments were performed with a variety of other compounds[50]. A soil sample that had been spiked with dimethyl methyl phosphonate (DMMP) was examined. and the spectrum agreed very well with the electron impact (EI) spectrum of DMMP with the exception of the molecular ion. The molecular ion is 34% of the base peak in the EI spectrum; in the laser desorption experiments, protonated DMMP is the base peak and the molecular ion is not observed. This again may be attributable to collisional processes occurring above the probe tip. Sensitivity for this analysis was excellent when compared with conventional mass spectral analyses.

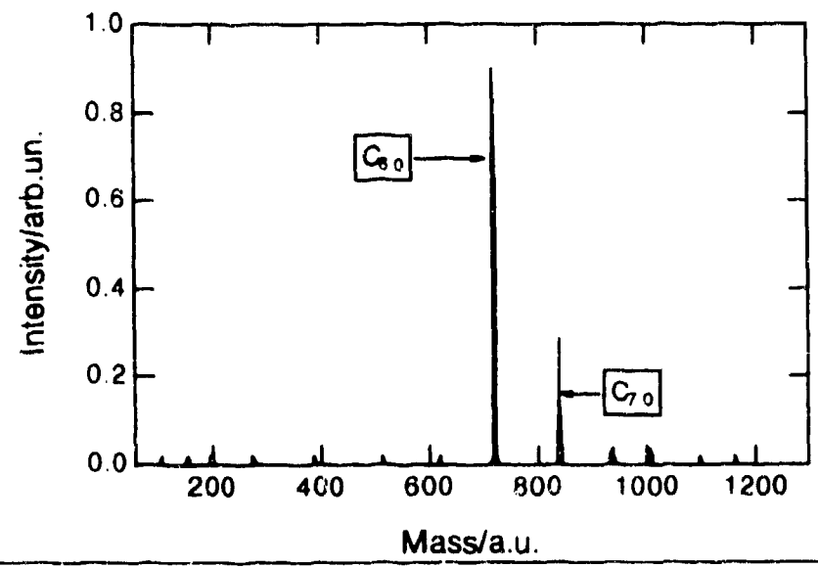

Figure 9 shows the positive ion spectrum obtained for laser desorption of sample containing several fullerene molecules.

The technique of alternate pulsed positive ion/pulsed negative ion mass spectrometry can be easily implemented with laser/ion trap instrumentation. Negative and positive ion signals can provide complementary data to determine the constituents of a complex mixture. Soot from a detonated mixture of trinitrotoluene and nitroguanidine (NIGU) was examined using both negative and positive ion mass spectra. The molecular ion of NIGU was observed almost exclusively in the negative ion mode whereas urea (a decomposition product from the explosion) is observed in the positive ion mass spectrum at m/z 60 along with several non-

diagnostic peaks at lower mass. These results agree very well with those obtained by thermal desorption direct-insertion probe mass spectrometry of this sample.

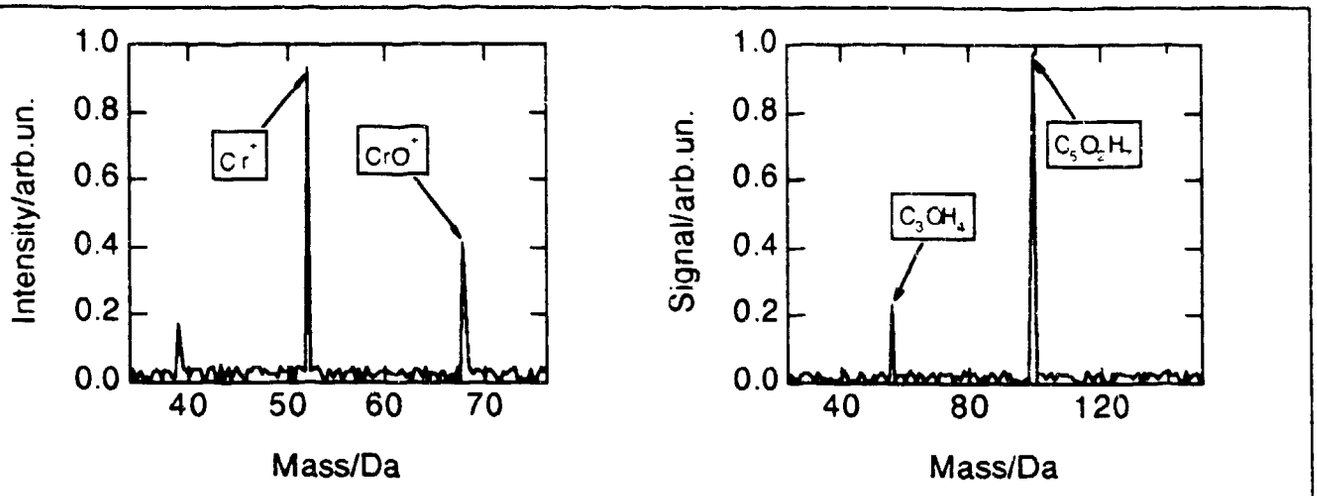

Figure 10. Shows the positive ion mass spectrum (left) obtained from high intensity laser desorption of chromium acetyl acetonate, and the negative ion mass spectrum (right) obtained under similar circumstances.

The complementary information provided by positive/negative ion laser desorption mass spectrometry can also be used to characterize transition metal complexes. The laser desorption positive ion mass spectrum of both nickel and chromium acetyl acetonate at 0.5 mJ/pulse shows primarily the molecular ion. Using higher laser energies (1.5 mJ/pulse), the complex was forced to decompose and elemental information could be obtained in the positive ion mode, Figure 10. By switching to negative ion mode at this laser energy, the intact acetyl acetonate negative ion was observed and could be interrogated with MS/MS techniques to yield structural information.

5. CONCLUSIONS

The combination of laser sampling and ion trap mass spectrometry promises to be a powerful analytical technique for the direct analysis of complex samples. The work presented here demonstrates that the sensitivity of this method can be increased significantly by improving the trapping efficiency. This increase is accomplished by firing the laser, and injecting ions into the trap, on the rising edge of the rf waveform, before the rf potential is fully developed. The rising rf field then insures that the ions remain trapped. In addition, our work in this field has demonstrated that the mass analysis of laser desorbed positive and negative ions provides complementary mass spectral information for mixture analysis: negative ion spectra emphasize organic content and molecular information, while the positive ion spectra yield useful structural and elemental information.

6. REFERENCES

1. R. J. Conzemius, J. M. Capellen, Int. J. Mass Spectrom. Ion Phys, **34**, 197, 1980.
2. E. Denoyer, G. R. Van, F. Adams, D. F. S. Natusch, Anal. Chem., **54**, 1982.
3. R. S. Houk, in *Analytical Applications of Lasers*, E. H. Peipmeier, Wiley, New York, (1986) 587.
4. R. J. Cotter, Anal. Chim. Acta, **195**, 45, 1987.
5. C. G. Gill, B. Daigle, M. W. Blades, Spectrochim. Acta, Part B, 46b, 1991.
6. B. Spengler, R. Kaufmann, Analusis, **20**, 91, 1992.
7. R. C. Estler, N. S. Nogar, J. Appl. Phys., **69**, 1654, 1991.
8. F. Hillenkamp, M. Karas, R. C. Beavis, B. T. Chait, Anal. Chem., **63**, 1193, 1991.

9. K. Dittrich, R. Wennrich, Prog. Anal. At. Spectrosc., **7**, 139, 1984.
10. L. Moenke-Blankenburg, *Laser Microanalysis*, Eds., John Wiley & Sons, New York, 1989.
11. C. R. Phipps, R. W. Dreyfus, in *Laser Ionization Mass Analysis*, A. Vertes, R. Gijbels, John Wiley and Sons, New York, (1992)
12. D. J. Burgess, P. C. Stair, E. Weitz, J. Vac. Sci. Technol., A, 1986.
13. N. S. Nogar, R. C. Estler, B. L. Fearey, C. M. Miller, S. W. Downey, Nucl. Instrum. Methods Phys. Res., Sect. B, **44**, 459, 1990.
14. M. R. Chevrier, R. J. Cotter, Rapid Commun. Mass Spectrom, **5**, 611, 1991.
15. T. B. Farmer, R. M. Caprioli, Biol. Mass Spectrom, **20**, 796, 1991.
16. J. A. Hill, R. S. Annan, K. Biemann, Rapid Commun. Mass Spectrom, **5**, 395, 1991.
17. R. S. Annan, H. J. Kochling, J. A. Hill, K. Biemann, Rapid Commun. Mass Spectrom, **6**, 298, 1992.
18. T. T. Yip, T. W. Hutchens, FEBS Lett, **308**, 149, 1992.
19. C. F. Llenes, R. M. O'Malley, Rapid Commun. Mass Spectrom, **6**, 564, 1992.
20. G. R. Parr, M. C. Fitzgerald, L. M. Smith, Rapid Commun. Mass Spectrom, **6**, 369, 1992.
21. E. D. Hardin, T. P. Fan, C. R. Blakley, M. L. Vestal, Anal. Chem., **56**, 2, 1984.
22. L. Ramaley, M. A. Vaughan, W. D. Jamieson, Anal. Chem., **57**, 353, 1985.
23. F. H. Strobel, T. Solouki, M. A. White, D. H. Russell, J. Am. Soc. Mass Spectrom, **2**, 91, 1991.
24. T. Solouki, D. H. Russell, Proc. Natl. Acad. Sci. U. S. A., **89**, 5701, 1992.
25. T. D. Wood, L. Schweikhard, A. G. Marshall, Anal. Chem., **64**, 1461, 1992.
26. X. Xiang, J. Dahlgren, W. P. Enlow, A. G. Marshall, Anal. Chem., **64**, 2862, 1992.
27. E. R. Grant, R. G. Cooks, Science, **250**, 61, 1990.
28. K. A. Cox, J. D. Williams, R. G. Cooks, R. E. J. Jaiser, Biol. Mass Spectrom, **21**, 226, 1992.
29. J. R. Gord, R. J. Bemish, B. S. Freiser, Int. J. Mass Spectrom. Ion Processes, **102**, 115, 1990.
30. R. R. Weller, T. J. MacMahon, B. S. Freiser, in *Lasers Mass Spectrom.*, Oxford, London, (1990) 249.
31. R. C. Dunbar, R. Klein, J. Am. Chem. Soc., **98**, 7994, 1976.
32. R. J. Hughes, R. E. March, A. B. Young, Int. J. Mass Spectrom. Ion Phys, **42**, 255, 1982.
33. R. J. Hughes, R. E. March, A. B. Young, Can. J. Chem., **61**, 824, 1983.
34. S. C. Beu, C. L. Hendrickson, V. H. Vartanian, D. A. J. Laude, Int. J. Mass Spectrom. Ion Processes, **113**, 59, 1992.
35. M. N. Kishore, P. K. Ghosh, Int. J. Mass Spectrom. Ion Phys, **29**, 345, 1979.
36. J. F. J. Todd, D. A. Freer, R. M. Waldren, Int. J. Mass Spectrom. Ion Phys, **36**, 371, 1980.
37. H. A. Schuessler, C. S. O, Nucl. Instrum. Methods Phys. Res., **186**, 219, 1981.
38. N. Watanabe, et al., Nucl. Instrum. Methods Phys. Res., Sect. B., **69**, 385, 1992.
39. D. N. Heller, I. Lys, R. J. Cotter, O. M. Uy, Anal. Chem., **61**, 1083, 1989.
40. G. L. Glish, D. E. Goeringer, K. G. Asano, S. A. McLuckey, Int. J. Mass Spectrom. Ion Processes, **94**, 15, 1989.
41. J. N. Louris, J. W. Amy, T. Y. Ridley, R. G. Cooks, Int. J. Mass Spectrom. Ion Process, **88**, 97, 1989.
42. J. M. Dale, W. B. Whitten, J. M. Ramsey, in *Laser Ablation*, J. C. Miller, R. F. Haglund, Springer-Verlag, New York, (1991) 344.
43. M. Lindinger, et al., Z. Phys. D., **20**, 441, 1991.
44. V. H. S. Kwong, Phys. Rev. A, **39**, 4451, 1989.
45. V. H. S. Kwong, Z. Fang, Y. Jiang, T. T. Gibbons, L. D. Gardner, Phys. Rev. A, **46**, 201, 1992.
46. A. McIntosh, T. Donovan, J. Brodbelt, Anal. Chem., **64**, 2079, 1992.
47. R. W. Kelly, R. W. Dreyfus, Nucl. Instr. and Meth., **B32**, 321, 1988.
48. R. Kelly, R. W. Dreyfus, Nucl. Instrum. Methods Phys. Res., **B32**, 341, 1988.
49. R. Kelly, J. Chem. Phys., **92**, 5047, 1990.
50. M. L. Alexander, P. H. Hemberger, M. E. Cisper, N. S. Nogar, Anal. Chem., submitted.